Journal of Manufacturing Processes 15 (2013) 41–50

Contents lists available at SciVerse ScienceDirect

Journal of Manufacturing Processes

journal homepage: www.elsevier.com/locate/manpro

Technical paper

Analytical model of metalworking fluid penetration into the flank contact zone in orthogonal cutting

Shibo Wang, Andres F. Clarens*

Civil and Environmental Engineering, University of Virginia, Charlottesville, VA, USA

ARTICLE INFO

Article history:
Received 29 January 2012
Received in revised form 20 July 2012
Accepted 27 September 2012
Available online 13 November 2012

Keywords:
Metalworking fluids
Minimum quantity lubrication
Reynolds equation
Supercritical carbon dioxide
Tool wear
Finite difference method
Finite element analysis

ABSTRACT

Metalworking fluids (MWFs) are used widely in machining process to dissipate heat, lubricate moving surfaces, and clear chips. They have also been linked to a number of environmental and worker health problems. To reduce these impacts, minimum quantity lubrication (MQL) sprays of MWF delivered in air or CO_2 have been proposed. MQL sprays can achieve performance comparable with conventional water-based or straight oil MWFs while only delivering a small fraction of the fluid. This performance advantage could be explained by the enhanced penetration into the cutting zone that results from delivering MWF in high pressure and precise sprays. To explore this hypothesis, an analytical model of MWF penetration into the flank face of the cutting zone is developed and validated using experimental data. The model is based on a derivation of the Navier–Stokes equation and the Reynolds equation for lubrication and applied to an orthogonal cutting geometry under steady-state conditions. A solution to the model is obtained using a numerical strategy of discretizing the analytical scheme with two-dimensional centered finite difference method. Penetration into the cutting zone is estimated for MQL sprays delivered in air, CO_2 and N_2 as well as two conventional MWFs, straight oil and semi-synthetic emulsion. The model suggests that conventional MWFs, do not penetrate the cutting zone fully and fail to provide direct cooling to the flank zone where wear is most likely to occur. MQL sprays do penetrate the cutting zone completely. Using convective heat transfer coefficients from a previous study, a finite element heat balance is carried out on the tool to understand how each fluid impacts temperature near the flank tip of the tool. The results of the modeling effort are consistent with experimental measurements of tool temperature during turning of titanium (6AL4V) using a K313 carbide tool. The prediction of temperature near the flank indicates that MQL sprays do suppress temperatures near the flank effectively. These results help explain the low levels of tool wear observed for some MQL sprays, particularly those based on high pressure CO_2. This modeling framework provides valuable insight into how lubricant delivery characteristics such as speed, viscosity, and cutting zone geometry can impact lubricant penetration.

1. Introduction

In orthogonal cutting operations,[1] metalworking fluids (MWFs) are typically applied from one of two directions to control heat and lubricate the interface between the tool and the workpiece (Fig. 1) [1,2]. The first of these is along the rake face of the tool where the chip and tool come into contact and where crater wear often develops [3]. This region is closest to the shear plane in the workpiece where the bulk of heat in metals machining is generated. Appreciable amounts of heat are also generated in this region by the friction between the chip and the tool. Here, MWF penetration occurs through a network of capillaries formed by scratches on the surface of the tool rake and the chip [4]. This contact area typically experiences extremely high pressures and temperatures such that conventional lubrication theory cannot be employed to explain fluid flow. Instead, previous studies have focused on understanding how MWF phase behavior (e.g., vapor pressure of lubricants) and machining conditions combine to produce the largely abrasive conditions under which crater wear develops [5].

The second contact zone into which MWFs must penetrate is the region between the workpiece and the flank face of the cutting tool. This region is important because flank wear can impact surface finish and tolerances on workpieces [6]. Since flank wear is largely a diffusive process driven by rubbing contact and heat accumulation in the cutting zone, MWF penetration is an important factor in controlling this form of tool wear [7]. The flank region of the cutting zone can be described as an inverted wedge with the heat source at the point of the wedge and the MWF entering through the open face at the bottom (Fig. 2). MWF spray direction can vary by operation, but when flank wear is a concern, lubricant is typically directed up into the flank contact zone from a nozzle placed directly below

* Corresponding author. Tel.: +1 434 924 7966; fax: +1 434 982 2951.
E-mail address: aclarens@virginia.edu (A.F. Clarens).

[1] All the units used in this research are SI units.

1526-6125/$ – see front matter © 2012 The Society of Manufacturing Engineers. Published by Elsevier Ltd. All rights reserved.
http://dx.doi.org/10.1016/j.jmapro.2012.09.015

Nomenclature

α	clearance angle between tool and workpiece
Θ_T	the process temperature
ρ	density of a viscous fluid
μ	viscosity of a fluid
c_1, c_2	integration constants
D	constant associated with the tool and work material
E	process activation energy
g_x, g_y	components of body force (gravitational) acceleration in x and y direction
G	abrasion rate, which is a function of cutting speed and feed
h	MWFs film thickness
i,j	labels in the two-dimensional finite difference method which correspond to x and y
L_y	characteristic length of tool flank
P	pressure inside MWFs
P_0	ambient pressure, $P_0 = 0$
R	the ideal gas constant
u_0	inlet velocity of MWFs
u_1, v_1 and w_1	components of workpiece velocity in x, y and z directions respectively
u_2, v_2 and w_2	components of tool flank velocity in x, y and z directions respectively
v_x, v_y and v_z	components of fluid velocity in x, y and z direction
x, y and z	three dimensions in the Cartesian coordinate system
z_0	total length of z dimension
$\Delta x, \Delta y$	mesh size of finite difference grid in x and y directions
$\frac{\partial h}{\partial y}, \frac{\partial h}{\partial z}$	first order derivative of h in y and z direction
$\frac{\partial P}{\partial x}, \frac{\partial P}{\partial y}$ and $\frac{\partial P}{\partial z}$	first order derivatives of P with respect to x, y and z respectively
$\frac{\partial v_x}{\partial x}, \frac{\partial v_x}{\partial y}$, and $\frac{\partial v_x}{\partial z}$	first order derivatives of v_x with respect to x, y and z respectively
$\frac{\partial v_y}{\partial x}, \frac{\partial v_y}{\partial y}$ and $\frac{\partial v_y}{\partial z}$	first order derivatives of v_y with respect to x, y and z respectively
$\frac{\partial^2 v_x}{\partial x^2}, \frac{\partial^2 v_x}{\partial y^2}$ and $\frac{\partial^2 v_x}{\partial z^2}$	second order derivatives of v_x with respect to x, y and z respectively
$\frac{\partial^2 v_y}{\partial x^2}, \frac{\partial^2 v_y}{\partial y^2}$ and $\frac{\partial^2 v_y}{\partial z^2}$	second order derivatives of v_y with respect to x, y and z respectively
$\frac{dW}{dt}$	wear rate over time

the tool [8]. Counteracting the lubricant penetration is the movement of the workpiece away from the cutting zone which tends to draw lubricants away from the tip of the wedge. The penetration of the lubricant into this region and how heat is removed and wear is controlled has not been explored in detail and is the focus of this research.

MWF penetration into the flank face of the cutting operation has become increasingly important with the advent of minimum quantity lubrication (MQL) technologies [9]. In an effort to reduce the occupational health and environmental impacts of MWFs, significant research and development efforts have been allocated toward developing MQL techniques [10,11]. These fluids deliver precise quantities of lubrication to the cutting zone eliminating the need for extensive infrastructure in the manufacturing facility [12]. When compared to conventional water-based MWFs, these new fluids tend to be less effective at removing heat, by virtue of their lower heat capacity [13]. In contrast, these MQL sprays tend to have lower

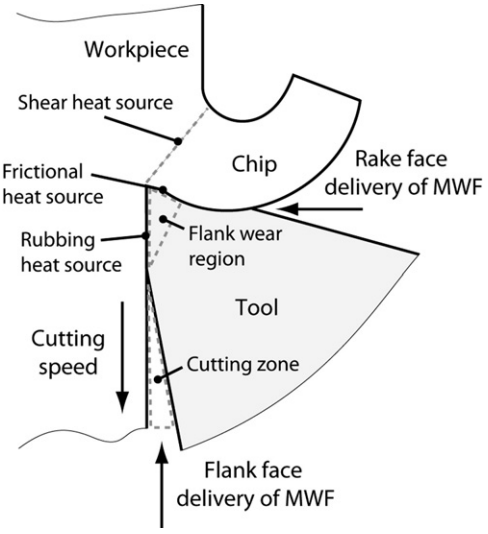

Fig. 1. Schematic of orthogonal cutting geometry showing sources of heat which can lead to abrasive wear in flank of tool. This wear is often controlled by applying MWF to the cutting zone.

viscosity and higher velocity suggesting that they might have an improved ability to penetrate the cutting zone [14]. Experimental results suggest that indeed, MQL sprays do effectively control tool wear more efficiently than could be predicted based on their heat removal capacity alone [15]. In particular, sprays of MWF based on compressed carbon dioxide control wear better than water-based fluids with a smaller fraction of the lubricant added [16]. The experimental results suggest that a combination of heat removal and penetration into the cutting zone is important in explaining the performance of these fluids [17]. These results reveal a key gap in the understanding of MWF penetration into the flank side of the tool of the cutting zone. The goal of this work is to provide a general model of MWF penetration into the flank cutting zone to inform MWF design and delivery.

The connection between temperature and tool wear has been well characterized for a number of metalworking operations [18]. For mild operations at low temperatures, abrasive wear tends to dominate. This type of wear can be controlled by applying adequate lubrication to the cutting zone. For more severe operations including turning of hard materials, diffusive wear tends to drive the wear process. For example, for tungsten–carbide–cobalt (WC–Co) tools, a large class of commonly-used tools, at high temperatures, the Co is able to move through the dislocations in the WC matrix. Wear can be predicted as an empirical function of temperature [19]:

$$\frac{dW}{dt} = De^{-E/R\Theta_T} \tag{1}$$

where D and E are diffusive rate constants that change depending on the tool, workpieces, and machining conditions. Under controlled conditions where D and E can be assumed to be constant, the wear rate is an exponential function of the inverse of tool temperature (Θ_T).

Recognizing that the behavior of MWF flow into the cutting zone could influence the temperature which induces tool wear, a modeling framework was needed to understand under which conditions enhanced penetration and heat removal is achieved. Fortunately, models of the hydrodynamics of lubricants are well described in the literature. The behavior of lubricant films in contact with moving solid surfaces has been studied extensively for over a century [20]. Driven by a need to ensure proper process function in rotating machinery and related processes, this work was focused on lubricant squeezed between sliders. The generalized Reynolds equation

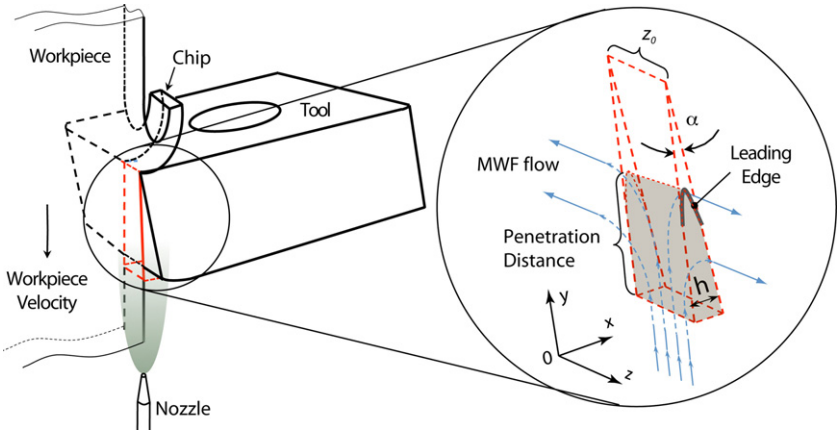

Fig. 2. 3-D representation of cutting tool and cutting zone and MWF penetration distance modeled here. All the derivations in this work follow the coordinate conventions here.

for lubrication, which forms the cornerstone of this work, can be applied much more generally to all hydrodynamic lubrication problems [21]. The Reynolds equation is based on the Navier–Stokes equation, and the continuity equation [22]. The model forms the basis for analytical modeling of lubricant fluid dynamics in which a thin film is moving between two solid plates [23]. To date the Reynolds equation has not been applied to the case of MWF penetration into the flank face between a tool and a workpiece. This paper develops an analytical equation, based on the Navier–Stokes equation and the Reynolds equation, to predict MWF dynamics in the contact zone for a range of applicable fluid and machining properties.

2. Modeling approach

The analytical framework developed here is derived from the Navier–Stokes equation and the Reynolds equation for lubrication. The Reynolds equation forms the cornerstone of quantitative treatment of hydrodynamic or elastohydrodynamic lubrication processes, i.e., where the distance between sliders is at least 3 nm [24]. The starting point for our derivation is the Navier–Stokes equation and the continuity equation for a three-dimensional Cartesian coordinate system which can be expressed as follows for an incompressible, laminar, and Newtonian flow [22]:

In the x direction:

$$\rho\left(\frac{\partial v_x}{\partial t}+v_x\frac{\partial v_x}{\partial x}+v_y\frac{\partial v_x}{\partial y}+v_z\frac{\partial v_x}{\partial z}\right) = \rho g_x+\mu\left(\frac{\partial^2 v_x}{\partial x^2}+\frac{\partial^2 v_x}{\partial y^2}+\frac{\partial^2 v_x}{\partial z^2}\right)-\frac{\partial P}{\partial x} \quad (2)$$

In the y direction:

$$\rho\left(\frac{\partial v_y}{\partial t}+v_x\frac{\partial v_y}{\partial x}+v_y\frac{\partial v_y}{\partial y}+v_z\frac{\partial v_y}{\partial z}\right) = \rho g_y+\mu\left(\frac{\partial^2 v_y}{\partial x^2}+\frac{\partial^2 v_y}{\partial y^2}+\frac{\partial^2 v_y}{\partial z^2}\right)-\frac{\partial P}{\partial y} \quad (3)$$

And the continuity equation is:

$$\frac{\partial v_x}{\partial x}+\frac{\partial v_y}{\partial y}+\frac{\partial v_z}{\partial z}=0 \quad (4)$$

Several simplifying assumptions are made to derive the Reynolds equation from the Navier–Stokes equation:

- Lubricant films are thin such that $h \ll L_y$. A dimensionless film thickness ratio is defined as $H = h/L_y$ and for hydroelastic lubrication $10^{-3} < H < 10^{-4}$ while for elastohydrodynamic lubrication $10^{-4} < H < 10^{-5}$ [24]. The Reynolds equation holds for both regimes.
- Lubricant flow is laminar. This is typically assessed using the Reynolds number (Re), which is a ratio of inertial forces to shear forces in the lubricant film. Since there is a significant velocity gradient between the two sliders, it is not appropriate to use h as the characteristic length when calculating the Reynolds number. Instead, a reduced Reynolds number is used where the Re is multiplied by H^2. The flows with reduced Reynolds numbers <1 are considered laminar.
- The pressure across the lubricant film is constant (i.e., $\partial P/\partial x = 0$). This assumption can be obtained by simplifying Eq. (2) and is reasonable for a wide range of lubricant conditions including laminar, turbulent, elastohydrodynamic, hydrodynamic, and others [25].
- No slip conditions at the interface between the solid and the lubricant. This is a common assumption in fluid dynamics when dealing with viscous fluids.
- No body forces influence the fluid. Body forces, such as gravity, are assumed to be small relative to the other forces acting on the lubricant.
- The lubricant is Newtonian. The response of a Newtonian fluid to shear stresses is proportional to the appropriate velocity gradient term.
- The lubricant has constant density, an assumption that is easily met by most incompressible lubricants.

Applying these assumptions to Eqs. (2)–(4) along with the continuity equation, the generalized Reynolds equation in two dimensions (y and z) can be written as [26]:

$$\frac{\partial}{\partial y}\left(\frac{h^3}{\mu}\cdot\frac{\partial P}{\partial y}\right)+\frac{\partial}{\partial z}\left(\frac{h^3}{\mu}\cdot\frac{\partial P}{\partial z}\right) = 6\frac{\partial h}{\partial y}(v_1-v_2)+6h\frac{\partial}{\partial y}(v_1+v_2) +6\frac{\partial h}{\partial z}(w_1-w_2)+6h\frac{\partial}{\partial z}(w_1+w_2)+12(u_1+u_2) \quad (5)$$

Fig. 3 presents (a) the general geometry for which the Reynolds equation was developed as well as (b) the geometry considered in this work. There are several important differences between the two systems. The most obvious is that for lubricated sliders modeled using the Reynolds equation, the lubricant is being drawn into the

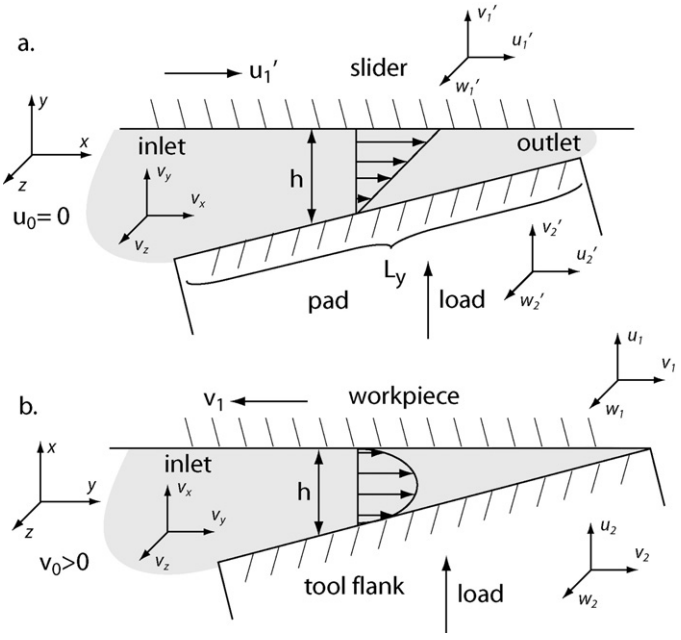

Fig. 3. Analogy between (a) geometry used in Reynolds equation and (b) geometry modeled here. All the derivations in this work are based on the geometry shown in (b).

contact zone by the relative movement of the solid surfaces. In machining, the opposite is true as the velocity of the work piece draws lubricant out of the cutting zone. In the Reynolds equation, the lubricant can exit the contact zone at the end whereas in machining, the contact between the tool and workpiece is not open. As a result, for the modeled system, the lubricant reaches a terminal velocity where it exits the wedge between the sliders in the z direction. This setup requires that the pressure inside the wedge be no higher than ambient pressure. In the Reynolds equation, a distinctive pressure gradient develops and is important in the derivation of a governing equation.

Several assumptions are needed to arrive at the Reynolds equation to apply it to MWF problems such that the conditions depicted in Fig. 3b can be modeled:

1. Metalworking fluids are incompressible. This is a valid assumption for conventional water-based fluids. It is less accurate for MQL, most of which are gas-based though the overall impacts on the model are negligible since here we assume that only small pressure gradient will exist. Since the lubricant is continuously replenished in the cutting zone, thermal expansion and other factors can be reasonably neglected.
2. Metalworking fluids are Newtonian fluids. Water, gases, and most lubricants (petroleum, biobased, and synthetic) are nominally Newtonian. The only possible violation of this assumption would be a metalworking fluid containing appreciable concentrations of surfactant, but the effect on the model would be expected to be small.
3. Metalworking fluids are laminar. This assumption was validated by calculating the reduced Reynolds number for each and confirming that for the velocities, viscosities, and characteristics lengths of interest, MWFs can be treated as laminar fluids.

In order to accurately capture the effects of MWF in orthogonal cutting, several modifications to the list of assumptions used to derive the Reynolds equation are proposed here. These are:

1. Since this is a steady state analysis, temporal variations in velocity are negligible such that $\partial v_{x,y,z}/\partial t = 0$. For most continuous cutting operations (e.g., turning) this is a reasonable assumption since depth of cut, feed rate, and cutting speed are typically kept constant during an operation.
2. MWFs are applied with a high initial velocity in the y direction, so the velocity in the x-axis is considered negligible ($v_x = 0$).
3. The body forces cannot be neglected in the y direction since gravity will slow the flow of MWF into the cutting zone assuming this is a vertically aligned cutting operation ($g_y = -g$, $g_x = 0$, $g_z = 0$). Over the length scales of interest, body forces were found to impact penetration distance between 3% and 8% and the leading edge position between 10% and 30%, a nontrivial amount that was incorporated into the final solution.

Since $v_2 = w_1 = w_2 = u_1 = u_2 = 0$, Eq. (5) is reduced to the general form of the Reynolds equation often shown in textbooks:

$$\frac{\partial}{\partial y}\left(\frac{h^3}{\mu}\cdot\frac{\partial P}{\partial y}\right) + \frac{\partial}{\partial z}\left(\frac{h^3}{\mu}\cdot\frac{\partial P}{\partial z}\right) = 6\frac{dh}{dy}v_1 \tag{6}$$

Eq. (5) is intractable both analytically and numerically, so a common simplification of this form of the Reynolds equation considers a specific geometry in which the characteristic length in the z-axis is much shorter than the characteristic length in the y-axis. This DuBois–Ocvirk approximation satisfies the following condition [26]:

$$\frac{\partial}{\partial y}\left(\frac{h^3}{\mu}\cdot\frac{\partial P}{\partial y}\right) \ll \frac{\partial}{\partial z}\left(\frac{h^3}{\mu}\cdot\frac{\partial P}{\partial z}\right) \tag{7}$$

In this work, the simplification is considered valid for the following condition:

$$\frac{(\partial/\partial y)((h^3/\mu)\cdot(\partial P/\partial y))}{(\partial/\partial z)((h^3/\mu)\cdot(\partial P/\partial z))} \leq 0.05 \tag{8}$$

In addition, the pressure gradient in the y direction is negligible when compared to the pressure gradient in the z direction such that only the shear flow in the y direction and the pressure flow in the z direction are taken into account. The resulting form of Eq. (6) is:

$$\frac{\partial}{\partial z}\left(\frac{h^3}{\mu}\cdot\frac{\partial P}{\partial z}\right) = 6\frac{dh}{dy}v_1 \tag{9}$$

Since the film thickness, h, in the cutting zone is a function of y which can be specified based on the cutting conditions, Eq. (9) simplifies to:

$$\frac{\partial^2 P}{\partial z^2} = \frac{6\mu v_1}{h^3}\cdot\frac{dh}{dy} \tag{10}$$

This second-order differential equation is then indefinitely integrated twice and rearranged to solve for pressure.

$$P(y,z) = \left(\frac{3\mu v_1}{h^3}\cdot\frac{dh}{dy}\right)z^2 + c_1 z + c_2 \tag{11}$$

where c_1 and c_2 are constants.

The boundary conditions needed to solve this differential equation are based on the pressure distribution that developed inside the cutting zone. As described earlier, the orthogonal cutting configuration is such that both sides of the cutting zone are open to the atmosphere. Therefore it is assumed that the boundary conditions (as shown in Fig. 2) are:

$$P = P_0 \text{ at } z = 0 \quad \text{and} \quad z = z_0$$

Solving for the constants c_1 and c_2 above yields:

$$c_1 = -\frac{3\mu v_1}{h^3}\cdot\frac{dh}{dy}\cdot z_0 \quad \text{and} \quad c_2 = 0 \tag{12}$$

Substituting these constants back into Eq. (10) provides an analytical solution for the pressure inside the cutting zone.

$$P(y,z) = \left(\frac{3\mu v_1}{h^3}\cdot\frac{dh}{dy}\right)(z^2 - z_0 z) \tag{13}$$

The resulting pressure gradient in the y direction is calculated by differentiating Eq. (13) with respect to y.

$$\frac{\partial P(y,z)}{\partial y} = -\frac{9\mu v_1}{h^4}(z^2 - z_0 z)\left(\frac{dh}{dy}\right)^2 \tag{14}$$

The pressure gradient presented in Eq. (14) can be substituted into Eq. (3) to obtain Eq. (15):

$$\rho v_y \frac{\partial v_y}{\partial y} = -\rho g + \mu\left(\frac{\partial^2 v_y}{\partial x^2} + \frac{\partial^2 v_y}{\partial y^2}\right) - \frac{\partial P}{\partial y} \tag{15}$$

and the resulting governing equation Eq. (16) provides the analytical description for MWF in the cutting zone:

$$\rho v_y \frac{\partial v_y}{\partial y} = -\rho g + \mu\left(\frac{\partial^2 v_y}{\partial x^2} + \frac{\partial^2 v_y}{\partial y^2}\right) + \frac{9\mu v_1}{h^4}(z^2 - z_0 z)\left(\frac{dh}{dt}\right)^2 \tag{16}$$

Eq. (16) can be rearranged to solve for velocity in the y direction:

$$v_y = \frac{-\rho g + \mu((\partial^2 v_y/\partial x^2) + (\partial^2 v_y/\partial y^2)) + (9\mu v_1/h^4)(z^2 - z_0 z)(dh/dy)^2}{\rho(\partial v_y/\partial y)} \tag{17}$$

3. Numerical solution

The velocity profile presented in Eq. (17) has no analytical solution. It can only be solved directly if the two second-order partial derivatives and the one first-order derivative are known. To solve it numerically, a two-dimensional centered finite difference method is used to discretize the geometry described in Fig. 3b. The derivatives are thus expressed as differences in the x and y directions, which can be made suitably small but finite. In effect, $v_y(x,y)$ is replaced by $v_y(i\Delta x, j\Delta y)$, which is further simplified as $v_y(i,j)$ [27].

In this manner, an arbitrary $v_y(i,j)$ can then be located with appropriate coordinates of i and j (Fig. 4).

This approach for solving Eq. (17) involves an inherent trade-off between precision and computational efficiency. For smaller finite differences, the results are more accurate but the computational time required to solve the equation becomes burdensome. Conversely, a more coarse mesh will result in truncation error that could lead to inaccurate results [28].

Using the finite difference method and applying a Taylor-series expansion to the derivative terms $\partial v_y(i,j)/\partial y$, $\partial^2 v_y(i,j)/\partial x^2$ and $\partial^2 v_y(i,j)/\partial y^2$, that appear in Eq. (17), approximations for each term are found to be:

$$\frac{\partial v_y(i,j)}{\partial y} = \frac{v_y(i,j+1) - v_y(i,j-1)}{2\Delta y} + O(\Delta y^2) \tag{18}$$

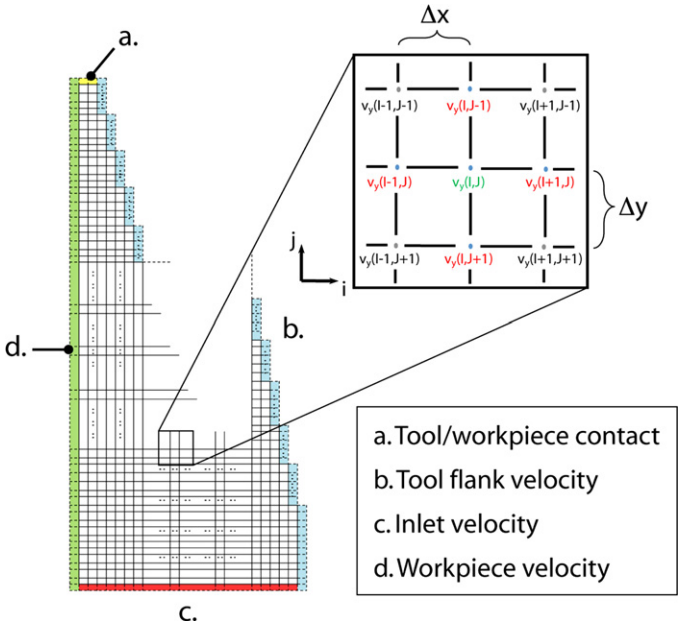

Fig. 4. Finite difference grid used to approximate solution to analytical equation of penetration model with boundary conditions regions labeled.

$$\frac{\partial^2 v_y(i,j)}{\partial y^2} = \frac{v_y(i,j+1) - 2v_y(i,j) + v_y(i,j-1)}{\Delta y^2} + O(\Delta y^2) \tag{19}$$

$$\frac{\partial^2 v_y(i,j)}{\partial x^2} = \frac{v_y(i+1,j) - 2v_y(i,j) + v_y(i-1,j)}{\Delta x^2} + O(\Delta y^2) \tag{20}$$

Substituting Eqs. (18)–(20) into Eq. (17), separating variables and combining like terms yields:

$$v_y(i,j) = \frac{-\rho g + \mu(((v_y(i+1,j) + v_y(i-1,j))/(\Delta x^2)) + ((v_y(i,j+1) + v_y(i,j-1))/(\Delta y^2))) + (9\mu v_1/h^4)(z^2 - z_0 z)(dh/dy)^2}{\rho((v_y(i,j+1) - v_y(i,j-1))/(2\Delta y)) + 2\mu((1/\Delta x^2) + (1/\Delta y^2))} \tag{21}$$

While Eq. (21) can be solved directly using the finite difference method, the consistency of the result is subject to variations in mesh size. This inconsistency was found to result from truncation error, which is amplified since it appears in both the numerator and denominator of Eq. (21). By rearranging Eq. (21) such that the truncation error is subtracted rather than divided, a more computationally stable governing equation can be found.

$$v_y(i,j) = \frac{-\rho g + \mu(((v_y(i+1,j) + v_y(i-1,j))/(\Delta x^2)) + ((v_y(i,j+1) + v_y(i,j-1))/(\Delta y^2))) + (9\mu v_1/h^4)(z^2 - z_0 z)(dh/dy)^2}{2\mu((1/\Delta x^2) + (1/\Delta y^2))} + \frac{\rho v_y(i,j)((v_y(i,j+1) - v_y(i,j-1))/(2\Delta y))}{2\mu((1/\Delta x^2) + (1/\Delta y^2))} \tag{22}$$

4. Modeling process

4.1. Computational scheme and boundary conditions

The nonlinear partial differential governing equation was solved using MATLAB® R2008a software package. The geometry of interest is defined for a representative tool insert. The inlet to the wedge region between the flank of the tool and the work piece is divided into 400 finite-difference cells, which for the cutting conditions modeled here corresponds to a length of $\Delta x = 1.04 \times 10^{-6}$ m. The length of Δy is chosen to be the same length in order to minimize numerical errors during the solution process. The fluids in the cells along the inlet to the wedge are assigned a velocity equivalent to the initial velocity of the MWF, which can be measured experimentally. The cells immediately adjacent to the workpiece

are assigned a velocity equivalent to the cutting speed of the operation, which can be specified. The fluid in the cells adjacent to the tool is assumed to have a velocity of zero. Since no fluid can pass the contact between the tool and the workpiece, the boundary condition is set at the contact between the tool and workpiece where there is a fluid velocity of zero. The fluid condition along the leading edge entering the wedge is a weak boundary condition since this position is ultimately the parameter to be calculated using the numerical method here. It is a weak boundary condition because it represents the transition from MWF to air. This boundary condition will exist for any fluid that does not penetrate the cutting zone fully.

4.2. Initial value specification

The centered finite difference method requires that an initial condition be specified to begin the calculations. A number of factors contribute to deceleration of the fluid within the cutting wedge including shear, gravity, and the constrained geometry of the cutting zone. The rate at which this deceleration happens depends on the specific geometry and conditions of the cutting operation and application rate of the MWF fluid. To account for this application specific effect, a deceleration coefficient is used. Small coefficients (suggesting rapid deceleration) led to spurious oscillations in the simulations. Consequently, the model was run at the first iteration assuming that the velocity of each subsequent cell was 0.75–0.99 the magnitude of the cell preceding it as shown in Eq. (23). This range is determined empirically and based on hundreds of trials and should represent a best estimate of the initial velocity. The exact value is cell-size dependent and case specific but it does not affect the steady-state result as long as the simulation converges to a steady-state value.

$$v_y(i,j) = (0.75\text{–}0.99)v_y(i,j-1) \tag{23}$$

For the purposes of setting the initial conditions, the distribution was uniform in the range described here and the initial condition was not found to impact the final results when selected from this range.

4.3. $\partial P/\partial y$ manipulation and interpolation

A solution to the analytical model proposed here must account for the pressure gradient that develops in the fluid. This $\partial P/\partial y$ term only exists in the part of the cutting zone that is filled with MWF and since the penetration was not known a priori, an iterative process was needed in which the equation was initially solved without the $\partial P/\partial y$ term and later added to refine the prediction. To improve this first estimate of the results, the body forces were also neglected at first since these would act in an opposite direction as the $\partial P/\partial y$ force. Gravity would cause the fluid to penetrate less into the wedge whereas the pressure gradient would induce additional penetration into the cutting zone. Since the $\partial P/\partial y$ term tends to be larger than body forces, after the first approximation, the penetration distance was reduced to 75% of the estimated value which was empirically determined to best reflect reality and re-run with the $\partial P/\partial y$ term and body forces included. This conservative reduction in penetration distance was determined empirically and since the model is recompiled after the entire governing equation is included, it does not affect the final result. This iterative process is more important for fluids with high initial velocities such as the MQL spray.

A satisfactory treatment of $\partial P/\partial y$ is one of the most significant modeling challenges associated with this analytical framework since the fluid does not always penetrate the entire cutting zone, e.g., for conventional MWFs. The location of the penetration distance can impact how the $\partial P/\partial y$ approximation is treated. If the 75% value exceeds the 0.05 cut-off value calculated using Eq. (8) (which is 2.75×10^{-3} m in this case), the values of the $\partial P/\partial y$ in finite difference cells below this cut-off are calculated following Eq. (14) while the above part is calculated using numerical interpolation strategy. This method to interpolate $\partial P/\partial y$ was developed specifically for fluids that do not penetrate the cutting zone completely using a Hermite interpolation technique [28]. The approximation is a function of the film thickness, h, which is a function of penetration distance y and the results closest to the flank wear region were found to be the most accurate.

4.4. Unified $\partial P/\partial y$ with respect to z

The pressure gradient that develops in the lubricant is an important factor in the Reynolds equation and as discussed earlier, it is included here even though the absolute pressure buildup is small since the cutting zone is open to the environment. According to Eq. (14), this pressure gradient changes in both the y and z directions. Numerical trials suggest, however, that some variation in $\partial P/\partial y$ exists in the z-axis with a maximum occurring near the center of the cutting zone. This variation is so small that $\partial P/\partial y$ can be reasonably considered to be independent of z. In this work, $\partial P/\partial y$ in the z direction is algorithmically averaged.

4.5. Leading edge criterion

A criterion for defining where the MWF has effectively stopped penetrating the cutting zone had to be specified before applying the numerical method. Since negative results do not make practical sense with respect to MWF velocity, negative values occurring within all the iterations are set to zero after each iteration. In this way, a clear boundary between velocities greater than zero and equal to zero emerges. For those cases where there are no negative values, the value of 10^{-5} m/s was selected as the criterion based on preliminary modeling work and the length scales involved. Velocities lower than this value were said to equal zero. The overall computational solution for the governing equation was derived using the flow chart shown in Fig. 5. Typically, 30,000–50,000 iterations are needed to acquire a convergent steady-state result.

4.6. Cutting conditions and MWF properties

The model was evaluated for the case of hard turning of titanium (6Al4V) using cutting conditions that are representative for a number of operations (speed = 0.762 m/s, feed rate = 2.03×10^{-4} m/revolution, and depth of cut = 1.27×10^{-4} m). This corresponds to a cutting speed of −0.7617 m/s. The negative values indicate that the velocity is in the opposite direction of the fluid flow. These values were selected to match experimental data the authors had collected in the laboratory. The K313 carbide tools were used because they are a commonly used tool material and the wear mechanisms that dominate in K313 are representative of other carbide types. For the purposes of developing an FEA (Finite Element Analysis) thermal model of the tool, the K313 was assumed to have a thermal conductivity of 2×10^4 W/m^2 °C based on literature from the manufacturer. The initial velocity of the fluids was calculated by measuring the volumetric flow rate of each MWF and dividing it by the cross-sectional area of the nozzle. For the CO_2 and N_2 sprays, the flow was approximated based on the literature since the velocity of these sprays can be supersonic near the nozzle [29]. The properties of the five MWFs evaluated here:

- *Emulsion flood* – A semi-synthetic MWF consisting primarily of water with surfactants and oil delivered from a modest pressure.
- *Straight oil/lubricant* – A lubricant stream applied to the cutting zone through a nozzle under slight pressure.

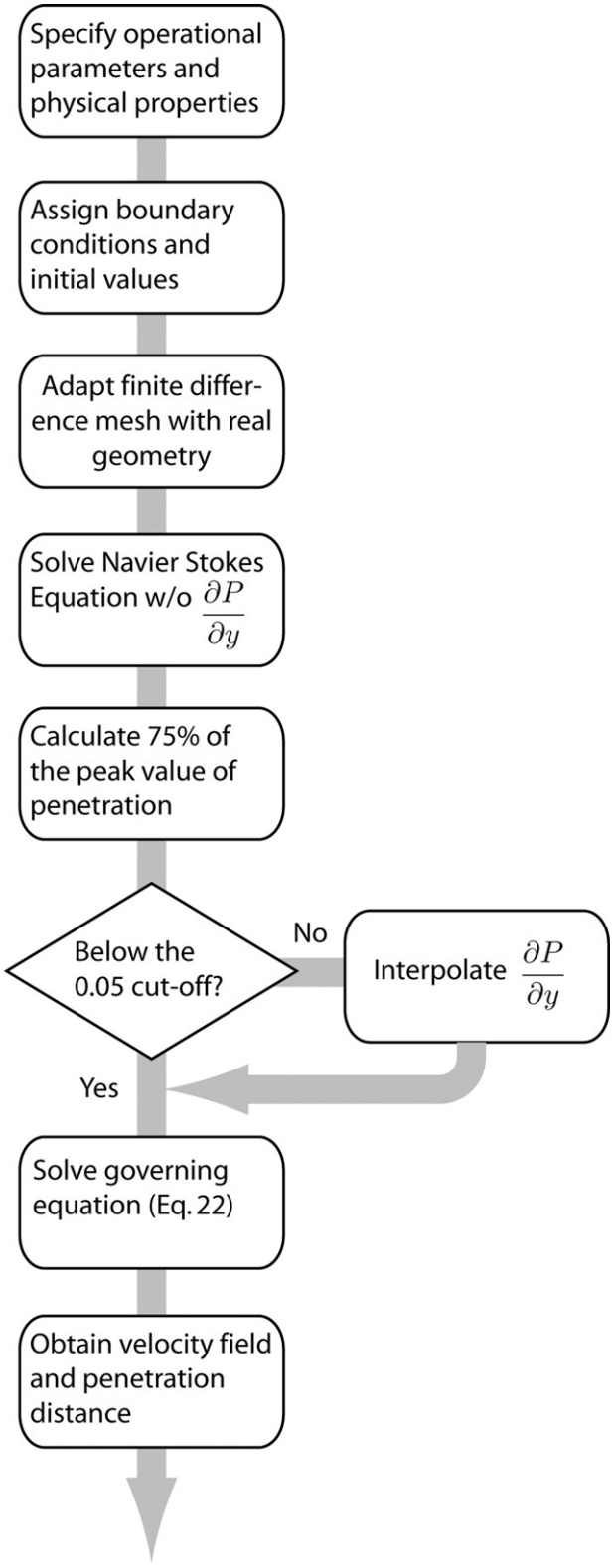

Fig. 5. Flowchart of algorithm used to solve numerical method applied here.

- *Emulsion spray* – A mist of emulsion MWF delivered using compressed air.
- *Supercritical carbon dioxide ($scCO_2$)* – Compressed carbon dioxide and dissolved carbon dioxide sprayed from high pressure to form dry ice and frozen lubricant droplets.

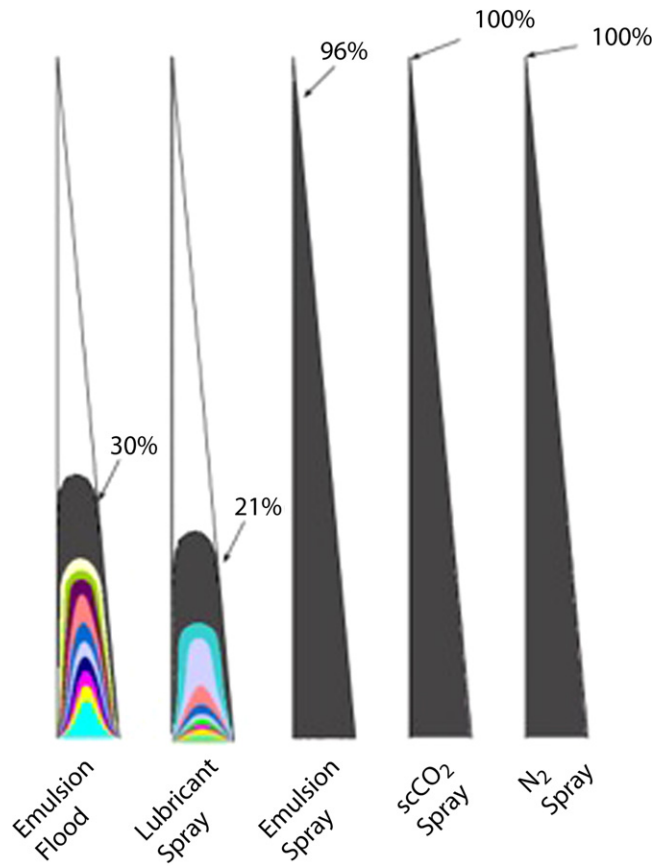

Fig. 6. Velocity contours (constant velocity lines) of MWF penetration into the cutting zone show significant differences in ultimate penetration distance (indicated with dotted lines for conventional MWFs since these do not penetrate near the end of the cutting zone).

- *High-pressure Nitrogen* – High pressure nitrogen delivered under conditions similar to the $scCO_2$ without the additional lubricant. Nitrogen also cools less effectively than carbon dioxide because of its Joule–Thomson properties.

The MWF modeling-relevant parameters are listed in Table 1.

5. Experimental model validation

The penetration of metalworking fluids into the cutting zone was estimated using the analytical model developed here and the results are presented in Fig. 6. As expected, the emulsion flood and the straight oil had significantly lower penetration into the cutting zone than the three environmentally adapted lubricants. This result is intuitive given the significantly higher viscosities and lower initial velocities of the water or oil based lubricants. The gas-based MQL penetrate the cutting zone completely.

In hard turning, MWF are used primarily to reduce temperature and control tool wear [31]. The improved penetration of MQLs suggests that they should have some advantage over conventional fluids when it comes to removing heat near the flank of the tool. But this difference must be evaluated in light of differences between convective heat removal of the different MWF systems. Gases have much lower molecular density than liquids and so their ability to dissipate heat will be lower. In earlier work, the authors measured the convective heat removal coefficient of the MWF systems described here under controlled conditions using a specialized probe [15]. These results, presented in Fig. 7, show that at low surface temperatures (<100 °C) the water-based fluids tend to remove

Table 1
MWFs evaluated in this work and their properties of interest.

MWF	Lubricant		Coolant		Inlet velocity (m/s)	Nozzle Radius (10^{-3} m)	Density (kg/m^3) [30]	Viscosity (Pa s) [30]
	Composition	Flow (g/s)	Composition	Flow (g/s)				
Emulsion flood	Petroleum semi-synthetic emulsion	0.05	Water	1	0.0535	2.5	1000 (4 °C)	0.00102 (20 °C)
Straight lubricant	Soybean oil	0.01	Air (6 bar)	1	0.0566	2.5	910	0.0455
Emulsion spray	Petroleum semi-synthetic emulsion	0.005	Air (6 bar) + water	1	16.454	1.27	1.2	1.8×10^{-5}
$scCO_2$ + lubricant	Soybean oil	0.001	Carbon dioxide (130 bar)	1	100	3.81	1.977	1.37×10^{-5}
Nitrogen	None	NA	Nitrogen (130 bar)	1	100	3.81	1.251	1.753×10^{-5}

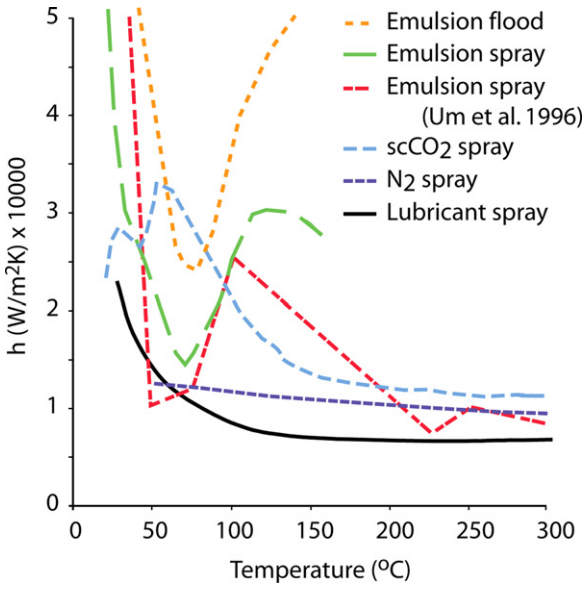

Fig. 7. Convective heat transfer coefficient for five different MWFs tested here. The experimental results are adapted from [15,32].

heat most effectively. At higher solid temperatures, however, the heat removal of the various MWFs is comparable with some (e.g., $scCO_2$) performing better than others (e.g., lubricant spray).

In order to integrate the results of Figs. 6 and 7 and produce an estimate tool flank temperature near the tip, a finite element model of the cutting zone was developed in ABAQUS® 6.7. The heat generation from cutting titanium was calculated using the method of heat generation described in [19]. Briefly, the heat in hard turning of titanium comes primarily from the shear zone where the chip is being created with a comparatively smaller amount of heat being generated where the tool rubs against the chip and where the tool rubs against the workpiece. The large majority of this heat enters the tool on the rake face and so the heat generation was applied to the finite elements of the tool on the rake face as shown in Fig. 8. MWF was applied to the flank of the tool using the penetration distances calculated in Fig. 6 and the convective heat transfer coefficients shown in Fig. 7.

The accuracy of the finite element model was assessed relative to direct measurements of temperature rise in the tool. A thermocouple was embedded beneath the tool near the base of the flank face. These measurements cannot provide a direct estimate of temperature at the flank since some fluid penetrate further into the cutting zone and direct measurement at the contact zone is notoriously challenging [33]. But these experimental results did provide a good means by which to calibrate the finite element model and in Fig. 9a, the experimental results are plotted along with modeling predictions of temperature rise in the tool. As shown here, the modeling results are highly consistent with experimental results.

The experimental temperature rise at the base of the tool and the temperature of the insert using the FEA model are shown in Fig. 9a. The data and the modeling results correspond well suggesting that the FEA model accurately predicts the heat generation associated with this cutting process. The temperature rise in the elements on the flank face of the cutting tool is shown in Fig. 9b. These results show a slightly different trend than the temperature at the base of the tool. At the base of the tool, the emulsion flood is the most effective at controlling the insert temperature. On the flank face of the tool, the emulsion flood is still effective, but the $scCO_2$-based spray is equally effective at removing heat from the tool. The temperature on the flank of the tool is emulsion flood (lowest temperature) $\approx$ $scCO_2$ + lubricant < emulsion spray < N_2 spray < straight lubricant. This suggests that a large part of the effectiveness of $scCO_2$-based MWF is due to its ability to penetrate the cutting zone and remove heat locally.

The temperature results in Fig. 9 were used to interpret experimental wear data of hard turning from the same experiments reported in [15]. These tool wear results showed that both $scCO_2$ + lubricant and emulsion flood had the lowest overall tool wear of the five different MWF tested. The results, presented in Fig. 10, show a clear correlation with the temperature

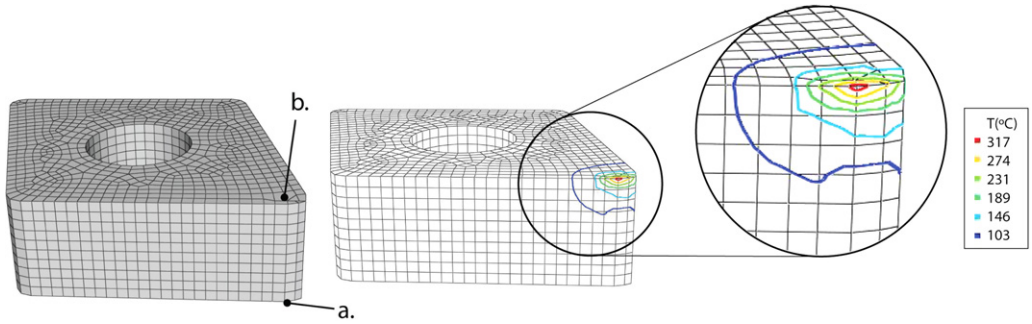

Fig. 8. Finite element model of tool showing the location of the two elements where temperature profiles were modeled over time (and plotted in Fig. 9) and the isotherms under steady state conditions.

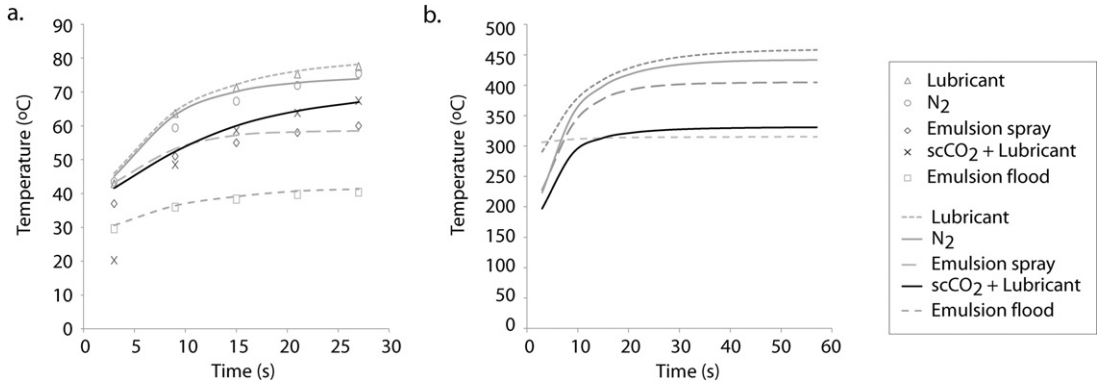

Fig. 9. Temperature rise in modeled K313 carbide tool when cutting titanium (6Al4V) on the (a) bottom of the tool showing both experimental and modeled results and (b) on the tool flank near the tip. The experimental results are adapted from [15].

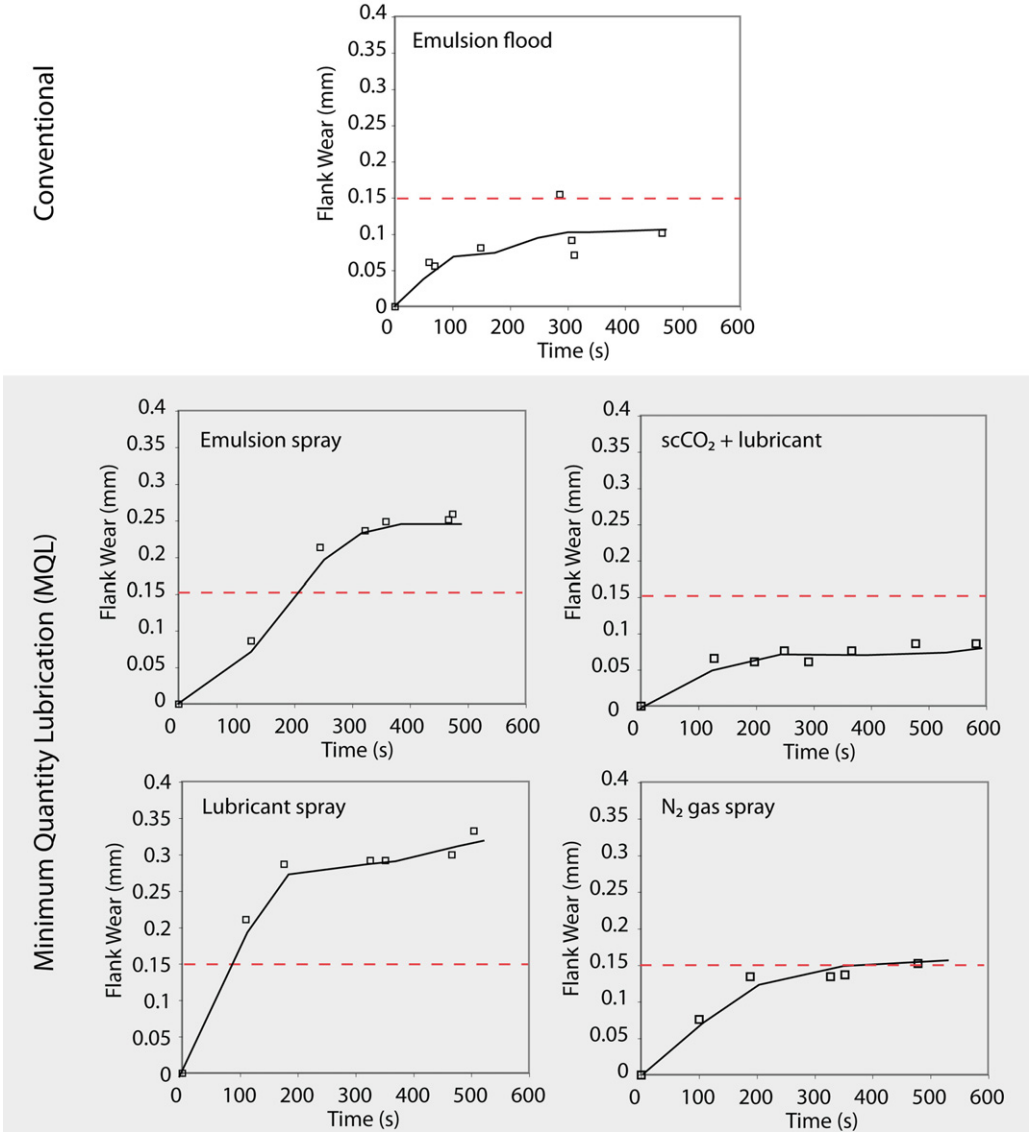

Fig. 10. Flank tool wear in the presence of different MWF when cutting titanium (6Al4V) using K313 carbide inserts. These results represent at least three replicates of each experiment. The experimental results are adapted from [15].

measurements of Fig. 9. The MWFs with the lower temperatures correspond to the lower levels of tool wear: emulsion flood (lowest level of wear) ≈ $scCO_2$ + lubricant < N_2 spray < emulsion spray < straight lubricant. It should be noted that N_2 spray resulted in higher tool temperature but less significant tool wear compared with emulsion spray. This is could be due to the inert chemical properties of N_2, which would limit metal oxidation. The wear rates in the presence of CO_2 are found to be 2 to 4 times lower than the other MQL alternatives after 300 s of cutting. Qualitatively, the tool wear in the presence of CO_2 produced fewer temperature discolorations suggesting a more uniform cooling was provided by CO_2. These results suggest that MQL, and specifically, CO_2-based coolants could become competitive with conventional MWF, not only because of their lower environmental profile, but because they control temperature, and by extension tool wear, more effectively than traditional MWFs. The results of this work provide a mechanistic understanding of how MWF penetration and heat removal can result in reduced tool wear.

6. Conclusions

An analytical framework for assessing metalworking fluid penetration into the flank cutting zone in orthogonal cutting is proposed based on the Navier–Stokes equation and a modified version of the Reynolds equation for lubrication. The numerical solution of the analytical framework is nontrivial and solved here using a centered finite difference numerical method. The model is used to evaluate the penetration of five different representative MWFs: emulsion, straight oil, emulsion mist, supercritical carbon dioxide with lubricant, and gaseous nitrogen. The penetration of the minimum quantity lubrication sprays was much higher than the conventional emulsion or straight oil.

These results help shed light on why some MQL sprays, such as those based on supercritical carbon dioxide, are able to control tool wear so effectively. To make the connection between penetration into the cutting zone and tool wear, a finite element model of the tool was developed. The model relied on experimentally measured convective heat transfer coefficients and tool temperature values measured at the base along with analytical estimates of heat production resulting from the cutting process and MWF penetration. The model effectively predicted the temperature rise in the tool that results from the cutting of 6Al4V titanium using a K313 carbide tool. The model also showed that temperature near the flank face of the cutting tool was most effectively controlled by MWF based on emulsions and $scCO_2$. This result corresponds directly with measurements of flank tool wear.

Acknowledgments

Financial support for this work came from NASA via a Virginia Space Grant Young Investigator Award and from faculty start-up funds from the School of Engineering and Applied Science at the University of Virginia. We thank Dong Liu from the University of Virginia for his assistance during model development.

References

[1] Byers J. Metalworking fluids. 2nd ed. New York: Marcel Dekker Inc.; 2006.
[2] Kishawy HA, Dumitrescu M, Ng E-G, Elbestawi MA. Effect of coolant strategy on tool performance, chip morphology and surface quality during high-speed machining of A356 aluminum alloy. International Journal of Machine Tools and Manufacture 2005;45:219–27.
[3] Al Huda M, Yamada K, Hosokawa A, Ueda T. Investigation of temperature at tool-chip interface in turning using two-color pyrometer. Journal of Manufacturing Science and Engineering, Transactions of the ASME 2002;124:200–7.
[4] Smith T, Naerheim Y, Lan MS. Theoretical analysis of cutting fluid interaction in machining. Tribology International 1988;21:239–47.
[5] Jiang H, Shivpuri R. A cobalt diffusion based model for predicting crater wear of carbide tools in machining titanium alloys. Journal of Manufacturing Science and Engineering, Transactions of the ASME 2005;127:136–44.
[6] Huang Y, Liang SY. Effect of cutting conditions on tool performance in CBN hard turning. Journal of Manufacturing Processes 2005;7:10–6.
[7] Li K-M, Liang SY. Modeling of cutting temperature in near dry machining. Journal of Manufacturing Science and Engineering, Transactions of the ASME 2006;128:416–24.
[8] Bittorf PJ, Kapoor SG, DeVor RE, Rajagopalan N. Effect of water phase surface tension and viscosity on metalworking fluid functionality. Milwaukee, WI: Society of Manufacturing Engineers; 2006. p. 555–62.
[9] Li K-M, Liang SY. Predictive models for flank wear in near dry machining. Orlando, FL: American Society of Mechanical Engineers; 2005. p. 49–57.
[10] Clarens AF, Zimmerman JB, Keoleian GA, Hayes KF, Skerlos SJ. Comparison of life cycle emissions and energy consumption for environmentally adapted metalworking fluid systems. Environmental Science and Technology 2008;42:8534–40.
[11] Furness R, Stoll A, Nordstrom G, Martini G, Johnson J, Loch T, et al. Minimum Quantity Lubrication (MQL) machining for complex powertrain components. Ypsilanti, MI: American Society of Mechanical Engineers; 2006. p. 9.
[12] Wang ZY, Rajurkar KP, Fan J, Petrescu G. Cryogenic machining of tantalum. Journal of Manufacturing Processes 2002;4:122–7.
[13] Ueda T, Hosokawa A, Yamada K. Effect of oil mist on tool temperature in cutting. Journal of Manufacturing Science and Engineering, Transactions of the ASME 2006;128:130–5.
[14] Dilip Jerold B, Pradeep Kumar M. Experimental investigation of turning AISI 1045 steel using cryogenic carbon dioxide as the cutting fluid. Journal of Manufacturing Processes 2011;13:113–9.
[15] Clarens AF, Park YE, Temme J, Hayes KF, Zhao F, Skerlos SJ. Evaluation of cooling potential and tool life in turning using metalworking fluids delivered in supercritical carbon dioxide. In: Manufacturing science and engineering conference (MSEC). West Lafayette, Indiana: ASME; 2009.
[16] Clarens AF, MacLean DF, Hayes KF, Park Y, Skerlos SJ. Solubility of a metalworking lubricant in high pressure CO_2 and effects in three machining processes. In: Society of manufacturing engineers. Dearborn 48121-0930, Clemson, SC, United States: Clemson University; 2009.
[17] Clarens AF, Hayes KF, Skerlos SJ. Feasibility of metalworking fluids delivered in supercritical carbon dioxide. Journal of Manufacturing Processes 2006;8:47–53.
[18] Mathew P. Use of predicted cutting temperatures in determining tool performance. International Journal of Machine Tools and Manufacture 1989;29:481–97.
[19] Shaw MC. Metal cutting principles. New York: Oxford University Press; 2005.
[20] Reynolds O. On the theory of lubrication and its application to Mr. Beauchamp tower's experiments. Philosophical Transactions of the Royal Society 1886;177:157–234.
[21] Wu L, Bogy DB. New first and second order slip models for the compressible Reynolds equation. Journal of Tribology 2003;125:558–61.
[22] Welty JR. Fundamentals of momentum, heat, and mass transfer. 3rd ed. New York: Wiley; 1984.
[23] Johansson L, Wettergren H. Computation of the pressure distribution in hydrodynamic bearings using Newton's method. Journal of Tribology 2004;126:404–6.
[24] Bhushan B. Introduction to tribology. New York: John Wiley & Sons; 2002.
[25] Szeri AZ. Fluid film lubrication: theory and design. Cambridge: Cambridge University Press; 1998.
[26] Hori Y. Hydrodynamic lubrication. Tokyo: Springer; 2006.
[27] Tannehill JC. Computational fluid mechanics and heat transfer. 2nd ed. Washington, DC: Taylor & Francis; 1997.
[28] Chapra SC. Applied numerical methods with MATLAB for engineers and scientists. 2nd ed. Boston: McGraw-Hill Higher Education; 2008.
[29] Franklin RK, Edwards JR, Chernyak Y, Gould RD, Henon F, Carbonell RG. Formation of perfluoropolyether coatings by the rapid expansion of supercritical solutions (RESS) process. Part 2: numerical modeling. Industrial and Engineering Chemistry Research 2001;40:6127–39.
[30] Lemmon EW, McLinden MO, Friend DG. Thermophysical properties of fluid systems. In: Mallard PJLaWG, editor. NIST chemistry WebBook. Gaithersburg, MD 20899: National Institute of Standards and Technology; 2010.
[31] Li K-M, Liang SY. Predictive modeling of flank wear in turning under flood cooling. Journal of Manufacturing Science and Engineering, Transactions of the ASME 2007;129:513–9.
[32] Um JY, Sehmbey MS, Chow LC. Thermal characteristics and critical heat flux behavior of cutting coolant and water mixtures under spray cooling. Atlanta, GA, USA; 1996. p. 185–91.
[33] Leshock CE, Shin YC. Investigation on cutting temperature in turning by a tool-work thermocouple technique. Journal of Manufacturing Science and Engineering 1997;119:502–8.